THE JOURNAL OF BIOLOGICAL CHEMISTRY VOL. 286, NO. 4, pp. 3065–3078, January 28, 2011

The C Terminus of Tubulin, a Versatile Partner for Cationic Molecules

BINDING OF TAU, POLYAMINES, AND CALCIUM[S]

Received for publication, May 12, 2010, and in revised form, October 11, 2010 Published, JBC Papers in Press, November 9, 2010, DOI 10.1074/jbc.M110.144089

Julien Lefèvre[1], **Konstantin G. Chernov, Vandana Joshi, Stéphanie Delga, Flavio Toma, David Pastré, Patrick A. Curmi**[2], **and Philippe Savarin**[3]

From the Laboratoire Structure-Activité des Biomolécules Normales et Pathologiques, INSERM-Université d'Evry-Val d'Essonne U829, Université Evry-Val d'Essonne, 91025 Evry, France

The C-terminal region of tubulin is involved in multiple aspects of the regulation of microtubule assembly. To elucidate the molecular mechanisms of this regulation, we study here, using different approaches, the interaction of Tau, spermine, and calcium, three representative partners of the tubulin C-terminal region, with a peptide composed of the last 42 residues of α1a-tubulin. The results show that their binding involves overlapping amino acid stretches in the C-terminal tubulin region: amino acid residues 421–441 for Tau, 430–432 and 444–451 for spermine, and 421–443 for calcium. Isothermal titration calorimetry, NMR, and cosedimentation experiments show that Tau and spermine have similar micromolar binding affinities, whereas their binding stoichiometry differs (C-terminal tubulin peptide/spermine stoichiometry 1:2, and C-terminal tubulin peptide/Tau stoichiometry 8:1). Interestingly, calcium, known as a negative regulator of microtubule assembly, can compete with the binding of Tau and spermine with the C-terminal domain of tubulin and with the positive effect of these two partners on microtubule assembly *in vitro*. This observation opens up the possibility that calcium may participate in the regulation of microtubule assembly *in vivo* through direct (still unknown) or indirect mechanism (displacement of microtubule partners). The functional importance of this part of tubulin was also underlined by the observation that an α-tubulin mutant deleted from the last 23 amino acid residues does not incorporate properly into the microtubule network of HeLa cells. Together, these results provide a structural basis for a better understanding of the complex interactions and putative competition of tubulin cationic partners with the C-terminal region of tubulin.

Microtubules are involved in a number of critical cellular processes, such as the determination of cell shape, chromosome segregation, intracellular transport of vesicles and organelles, and cell migration. Microtubules consist mainly of αβ-tubulin heterodimers organized head-to-tail into protofilaments whose parallel self-association gives rise to microtubules (1–4). α- and β-tubulin monomers have each a molecular mass of 50 kDa and are organized in three domains, namely the N-terminal domain (amino acid residues 1–205) involved in nucleotide binding, the intermediate domain (amino acid residues 206–384), and the C-terminal domain (amino acid residue 385 to the C terminus) (5). The C-terminal domain of tubulin represents a critical part of the binding site of different tubulin/microtubules partners, such as MAPs,[4] which are major regulators of microtubule dynamics (6–8), or polycations, which promote tubulin assembly *in vitro* in different polymeric forms (9). The C-terminal domain comprises a highly negatively charged tail of about 20 amino acid residues (named herein the C-terminal tail (CTT)), which protrudes from the surface of microtubules. In agreement with its participation in the regulation of microtubule assembly through interactions with partners, the CTT is also the most divergent part of tubulin, and variations among tubulin isotypes (10) may explain the modulation of the dynamics of microtubule assembly in specific tissues or cytoplasmic regions.

Different structure information has been obtained regarding the C-terminal domain of tubulin by using either full-length tubulin or peptide fragments. Electron crystallography of zinc-induced tubulin sheets showed the presence of two anti-parallel α-helices (helix H11 (amino acid residues 385–397) and helix H12 (amino acid residues 418–433)) lying at the outer surface of tubulin. The regions corresponding to the CTTs of either α- or β-tubulin were however not observed, probably due to the flexibility of this part of the protein (5). These observations were confirmed by x-ray diffraction analyses of crystal complexes formed between tubulin and the RB3-stathmin-like domain (11–13). Other structural data were obtained with peptides from the C-terminal region of tubulin studied either when free in solution or in interaction with different partners. NMR structure investigations on α- and β-tubulin C-terminal peptides showed that both α (residues 404–451) and β (residues 394–445) peptides have no defined secondary structure in aqueous solution but contain a well

[S] The on-line version of this article (available at http://www.jbc.org) contains supplemental Table 1 and Figs. 1–4.

[1] Recipient of a postdoctoral fellowship (NeRF) from Le Conseil Régional d'Ile-de-France.

[2] To whom correspondence may be addressed. Tel.: 33-1-69-47-01-87; E-mail: pcurmi@univ-evry.fr.

[3] To whom correspondence may be addressed. Tel.: 33-1-69-47-01-69; E-mail: philippe.savarin@univ-evry.fr.

[4] The abbreviations used are: MAP, microtubule-associated protein; αTub410C, amino acid residues 410–451 from α1a-tubulin; CTT, tubulin C-terminal tail; ITC, isothermal titration calorimetry; tubulin S, subtilisin-treated tubulin; EGFP, enhanced green fluorescent protein; CNS, central nervous system.

defined central helix region surrounded by disordered N and C segments in the presence of 30% trifluoroethanol. Helices span residues 418–432 and 410–432 for α- and β-tubulin, respectively (14). Both α- and β-C-terminal domains of tubulin were demonstrated to interact with MAP2, Tau (15, 16), and MAP4 (17, 18). More recently, the NMR solution structure of the Cap-Gly-2 domain of the CLIP-170 protein in complex with a C-terminal α3-tubulin peptide (residues 416–451) was obtained (19). It was found that the region of this peptide corresponding to the CTT is critical for this interaction because the acidic motif (residues 447–450) of the α-tubulin tail interacts with the basic groove of the Cap-Gly-2 domain and because the C-terminal end residue Tyr^{451} is anchored to a hydrophobic patch of the basic Cap-Gly-2 groove. The remainder of the α3-tubulin peptide was found largely disordered.

Finally, numerous studies showed that small cationic molecules and cations could interact with tubulin C-terminal tails. Among small cationic molecules are polyamines, such as tetravalent spermine, trivalent spermidine, and their diamine precursor, putrescine, which are also known as key modulators of cell growth. *In vitro*, polyamines promote microtubule assembly with an efficiency proportional to the number of free amino groups that they bear. Spermine (Table 1*A*), with four amino groups, is the most effective polyamine already tested in this respect (20). *In vivo*, a recent study concerning the relationships between polyamine levels and microtubule assembly in a cellular context showed that polyamines are potential regulators of the complex dynamical properties of the microtubules network (21).

Regarding calcium, which behaves as a powerful direct or indirect (via MAPs (22)) microtubule-destabilizing agent (23, 24), the presence of a high affinity binding site located in the C-terminal region around amino acid residues α423–446 and β404–427 has been demonstrated (25), but the atomic characterization of this binding site has never been determined.

More detailed knowledge on structure-activity relationship concerning the C-terminal part of tubulin will provide a better understanding of physiological regulations and help to develop novel approaches to target microtubule dynamics. It is noteworthy that, due to its high negative charge, the C-terminal domain of tubulin interacts mainly with cationic partners of different natures: proteins, small molecules, or cations. This suggests that an interplay might exist between various cationic tubulin partners and physiological consequences in living cells. In this context, the aim of the present work was to characterize the NMR solution structure of an α1-tubulin C-terminal peptide, which comprises helix H12 and the CTT (amino acid residues 410–451, named herein αTub410C), and to study by different means its interaction with Tau, spermine, putrescine, and calcium chosen as representative members of tubulin cationic partners. The results confirm the absence of structure of this peptide in aqueous solution and indicate some overlaps in the binding regions of Tau, spermine, and calcium. Interestingly, we demonstrate that Tau and spermine compete for αTub410C binding and that calcium can displace both of these molecules from the αTub410C peptide. Such a competition may explain in part how calcium can impede microtubule assembly in the physiological context. Finally, we found that a part of the C-terminal tubulin domain is needed for the correct incorporation of α-tubulin into microtubules in HeLa cells underlying its importance in the regulation of microtubule dynamics.

MATERIALS AND METHODS

Production and Purification of the α1-Tubulin αTub410C Peptide—As a first approach, we attempted to express the full-length tubulin C-terminal domain. Unfortunately, this yielded insoluble material. We further expressed a peptide starting at residue 398 (just after the end of helix H11), but it was again insoluble. We finally succeeded in expressing and purifying a soluble form of a peptide that comprises the last 42 C-terminal residues of the human α1a-tubulin (amino acid residues 410–451, named herein αTub410C (Table 1*B*)). It was expressed in recombinant form as a fusion peptide with an N-terminal polyhistidine tag. The αTub410C cDNA was amplified by PCR using the pEGFP-Tub plasmid as template (BD Biosciences Clontech, catalogue no. 632349). The upstream and downstream primers contained NdeI and BamHI sites, respectively, to insert the PCR product into the pET16b plasmid. Fidelity of PCR amplification and phase were verified by sequencing (Cogenics, Brea, CA).

E. coli BL21 DE3 Gold cells (Invitrogen) harboring the plasmid coding for αTub410C were grown at 37 °C with 100 μg/ml ampicillin in a 1-liter flask of LB medium or isotopically labeled M9 minimal medium containing 0.6 g/liter 95% $^{15}NH_4Cl$ and 2.2 g/liter 95% ^{13}C-glucose (Cortecnet, Paris, France) as the sole nitrogen and carbon sources, respectively, and complemented with 1 mg/liter thiamine and 1 mg/liter biotin. Peptide expression was induced at $A_{600\ nm} = 0.5$ with 1 mM isopropyl β-D-thiogalactopyranoside, and incubation was continued at 37 °C for 3.5 h. Bacteria were pelleted by a 10-min, 4,000 × *g* centrifugation, and the pellet was resuspended in 10 volumes of Buffer A (20 mM Tris-HCl, pH 7.6, 100 mM NaCl). Bacteria were then disrupted by sonication, and the product was centrifuged for 30 min at 100,000 × *g* at 4 °C. Clarified cell lysate was then loaded on an Ni^{2+}-nitrilotriacetic acid column (Qiagen, Hilden, Germany) equilibrated with Buffer A. The proteins were eluted with 5 column volumes of buffer B (20 mM Tris-HCl, pH 7.6, 100 mM NaCl, 300 mM imidazole). The fractions containing the αTub410C were combined and concentrated by ultrafiltration (Amicon, 5 kDa cut-off) to 0.5 ml at 4 °C and diluted into 4.5 ml of buffer C (20 mM MES-KOH, pH 6.9). The procedure of concentration/dilution was repeated again three times with buffer C to eliminate traces of imidazole. The final concentration of αTub410C was determined by amino acid analysis. The result was used to determine the extinction coefficient of αTub410C for further analyses ($\epsilon_{205\ nm} = 3.56 \times 10^5\ M^{-1}\ cm^{-1}$). The final yield was about 2 mg/liter pure peptide. All of the purification steps were performed in the presence of protease inhibitor mixture (Roche Applied Science) at room temperature except for the centrifugation and the concentration steps (4 °C).

Production of Full-length Human Tau Protein—E. coli BL21 DE3 Gold competent cells were transformed with the hTau40

pET29b plasmid (catalogue no. 16316, Addgene, Cambridge, MA). Bacteria were grown in LB medium in the presence of 100 μg/ml ampicillin. Overexpression was induced at $A_{600\ nm} = 0.5$ with 1 mM isopropyl β-D-thiogalactopyranoside, and incubation was continued for 3.5 h at 37 °C. After collection of bacteria by centrifugation as described above, pellets were dissolved in 10 ml of 50 mM MES-KOH, pH 6.9, 500 mM NaCl, 1 mM $MgCl_2$, and 5 mM DTT and then sonicated and centrifuged for 10 min (4,000 × *g*). The supernatant was boiled for 20 min, and the lysate was then ultracentrifuged at 100,000 × *g* for 45 min. The soluble hTau40 fractions were concentrated by ultrafiltration (Amicon, 10 kDa cut-off), and the protein was diluted in 20 mM MES-KOH, pH 6.9, 5 mM NaCl, 1 mM DTT. The final concentration of hTau40 was determined by amino acid analysis.

Preparation of Sheep Brain Tubulin and Subtilisin-treated Tubulin—Tubulin was purified from sheep brain using the method of Castoldi and Popov (26) and stored at −80 °C in 20 mM MES-KOH, pH 6.9, 0.5 mM DTT, 0.5 mM EGTA, 0.25 mM $MgCl_2$, 3.4 M glycerol, and 0.1 mM GTP. Before use, an additional cycle of polymerization was performed, and tubulin was resuspended in 20 mM MES-KOH, pH 6.9, 0.25 mM EGTA, 0.25 mM $MgCl_2$. Subtilisin-treated tubulin (tubulin S) was prepared using a standard protocol (27). Tubulin and tubulin S concentrations were determined by spectrophotometry using an extinction coefficient $\epsilon_{278\ nm} = 1.2 \times 10^5\ M^{-1}\ cm^{-1}$ (28).

NMR Experiments—NMR spectra were acquired at 20 °C on a Bruker Avance 600 NMR spectrometer using a triple resonance cryoprobe equipped with *z* axis self-shielded gradient coils. All experiments were performed on 60-μl samples with the MATCH^{TM} system (Cortecnet). NOESY- and TOCSY-^{1}H-^{15}N HSQC experiments were collected on a 400 μM ^{15}N-labeled αTub410C peptide sample. Three-dimensional HNCA, HNCACB, and CBCA(CO)NH experiments were performed to check and facilitate backbone assignments on a 400 μM ^{15}N-^{13}C-labeled αTub410C peptide sample (29). The spectra were acquired with 1024 complex data points in the direct dimension and 24 × 60 complex data points in the N and C dimensions, respectively. The spectral widths were 8992 Hz (^{1}H), 1650 Hz (^{15}N), 9433 Hz (^{13}Cα, ^{13}Cβ), and 3750 Hz (^{13}Cα). All acquired spectra were processed with Topspin 2.0 and NMRView (30). Visualization and manipulation were performed with NMRView (freeware version).

Two-dimensional ^{1}H-^{15}N HSQC experiments were used to perform the spermine and Ca^{2+} titration series using a 200 μM ^{15}N-labeled αTub410C peptide sample dissolved in 20 mM MES-KOH, pH 6.9. The spectra were recorded using 256 × 1024 complex data points in F1 and F2 dimensions with 16 scans/increment and a relaxation delay of 1.2 s. The spectral widths were 1650 and 2000 Hz in the ^{15}N and ^{1}H dimensions, respectively. Titrations were performed by the stepwise addition of 2 μl of concentrated stock solutions of polyamines or calcium prepared as chloride salts. One NOESY-^{1}H-^{15}N HSQC spectrum was recorded in the presence of 400 μM ^{15}N-labeled αTub410C and 3 mM spermine. For titration with Tau, a sample of 80 μM ^{15}N-labeled αTub410C peptide in 20 mM MES-KOH, pH 6.9, in the presence of 1 mM DTT was prepared. Tau was then added at a concentration of 10 μM. Mean weighted chemical shift displacements (Figs. 2*B* and 4*C*) were calculated according to the formula, $((\Delta\delta^1H)^2 + (\Delta\delta^{15}N)^2/6.5^2)^{1/2}$ (31). The significant threshold was calculated for each curve as the mean chemical shift deviation multiplied by 1.5.

For one-dimensional NMR tubulin or titration experiments, 40 μM tubulin in 20 mM MES-KOH, pH 6.9, 2 mM $MgCl_2$, 20% glycerol was incubated in the presence of increasing concentrations of spermine or putrescine. At the end of the experiment, 500 mM KCl or an increasing concentration of Ca^{2+} was added to the sample. Intensities of the spectra were calibrated with an external reference.

For two-dimensional NMR Tau/spermine competition experiments, a sample containing 100 μM ^{15}N-labeled αTub410C peptide was prepared in 20 mM MES-KOH, pH 6.9, 1 mM DTT. Increasing amounts of Tau or spermine were added up to 40 μM and 9 mM, respectively.

Isothermal Titration Calorimetry (ITC)—ITC measurements were performed at 25 °C using a MicroCal VP titration calorimeter (MicroCal Inc., Northampton, MA). Samples were thoroughly degassed before each titration. Titration and sample solutions were made up in the same buffer solution (20 mM MES-KOH, pH 6.9). Titrations were carried out by injecting 32–55 consecutive aliquots (5–10 μl) of ligands at different concentrations into the ITC cell (1-ml volume) containing the αTub410C peptide. For spermine/putrescine experiments, injections were carried out at 340-s intervals. The best titration curves were obtained using 1.5 mM spermine into the syringe and 11 μM αTub410C peptide into the cell. For hTau40 experiments, injections were carried out at 240-s intervals. Best titration curves were obtained with 22 μM hTau40 into the syringe and 8 μM αTub410C peptide into the cell. A background titration consisting of the identical titration solution but containing only the buffer in the cell was subtracted from each titration to account for heat produced by sample dilution. The value obtained was subtracted from the heat of reaction to give the effective heat of binding. The resulting titration data were analyzed using the ORIGIN software package supplied by MicroCal. The molar binding stoichiometry (*N*), binding constants (K_a; $K_d = 1/K_a$), and binding enthalpy (ΔH) were determined by fitting the binding isotherm to a model with one set of sites. For the fit, no constraint in stoichiometry, K_a, and ΔH was fixed. Changes in free energy (ΔG) and in entropy ($T\Delta S$) were calculated from $\Delta G = -RT \ln K_a = \Delta H - T\Delta S$, where *R* is the gas constant and *T* is the temperature in Kelvin. All values are the average of three experiments ± S.D. Errors in $T\Delta S$ values were calculated by the equation, $(S.D.^2(\Delta H) + S.D.^2(\Delta G))^{1/2}$.

In Vitro Polymerization Assay—Tubulin polymerization was monitored turbidimetrically at 350 nm (1-cm path) in an Ultrospec 3000 spectrophotometer (GE Healthcare) equipped with a temperature controller. Experiments were carried out using 30 μM tubulin in 20 mM MES-KOH, pH 6.9, 2 mM $MgCl_2$, and 1 mM GTP with 25% glycerol at 37 °C. Tau, spermine, and calcium were added at varying concentrations, as indicated in the figures. Tau experiments were performed

in the presence of 1 mM DTT except when probing oxidative conditions.

Tau-Spermine-Microtubule Co-sedimentation Experiments—To work only with functional proteins, 40 μM tubulin together with 50 μM Tau was polymerized at 37 °C for 10 min in 40 mM MES-KOH, pH 6.9, 1 mM GTP, 1 mM DTT, 4 mM $MgCl_2$. After mild centrifugation to collect microtubules only (25,000 × *g*, 15 min at 37 °C), the supernatant was discarded, and the microtubule pellet containing Tau was resuspended in the same buffer and depolymerized at 4 °C for 10 min and then separated in three aliquots to which 30 μl of buffer without (control) or with concentrated spermine was added to reach 1 and 3 mM spermine final concentration. Aliquots were then returned to 37 °C for 15 min and centrifuged (25,000 × *g*, 15 min, 37 °C). Supernatant and pellet were finally analyzed by 12% SDS-PAGE.

Cell Culture, Transfection, and Fluorescence Microscopy—The pEGFP-Tub plasmid encodes a fusion protein of green fluorescent protein (EGFP) and the cDNA encoding human α-tubulin (GFP-Tub). Plasmids derived from pEGFP-Tub encode the EGFP-α-tubulin fusion protein with a deletion of the 23 last C-terminal amino acid residues (GFP-TubΔ23C) and of the 13 last C-terminal residues (GFP-TubΔ13C) of the human α-tubulin. Plasmids were constructed by PCR using the plasmid pEGFP-Tub as template and the primers 5′-ACCTCGATATCGAGCGCCCA-3′ and 5′-ATCCGGATCCTTAAAGGGCAGCCATATCTTCACG-3′ for pEGP-TubΔ23C and 5′-ACCTCGATATCGAGCGCCCA-3′ and 5′-ATCCGGATCCTTAATCCACACCAACCTCCTC-3′ for pEGFP-TubΔC13 (*Eco*RV and *Bam*HI sites have been underlined). The PCR products corresponding to C-terminal deleted tubulin were cloned in frame with EGFP into the plasmid pEGFP-tub using EcoRV and BamHI sites. Sequences and phases of the inserts were verified by DNA sequencing (Cogenics).

HeLa cells were grown on glass coverslips in 4-well plates at 37 °C with 5% CO_2 in DMEM containing 10% fetal bovine serum and 1% penicillin/streptomycin. Transfections with the pEGFP-Tub, pEGFP-Tub-ΔC13, or pEGFP-Tub-ΔC23 plasmids were performed as follows. Fresh culture medium without serum was added to the cells before transfections. 0.2 μg of plasmid DNA was used for 1 μl of Lipofectamine, both of them diluted in 40 μl of Opti-MEM I (Invitrogen protocol). DNA-Lipofectamine mix was left for 20 min at room temperature and then added to the cells and gently mixed. Cells were returned to the incubator at 37 °C. 4 h post-transfection, the medium was replaced with fresh full medium, and cells were incubated for 24 h at 37 °C. When necessary, 0.5 μM taxol was added for 1 h. Cells were washed twice with PBS and fixed/permeabilized with methanol at −20 °C for 20 min. Cells were then incubated for 30 min at 37 °C with the blocking solution (20 mM Tris-HCl, pH 7.4, 150 mM NaCl, 0.1% Triton, 2% BSA, 0.1% NaN_3). The microtubule network was labeled for immunofluorescence with the E7 anti-tubulin mouse monoclonal antibody diluted at 1:5000 in blocking solution overnight at 4 °C. Cells were washed twice with PBS and incubated with goat anti-mouse antibody (Alexafluor 555) diluted at 1:2500 in blocking solution for 1 h at room temperature. The cells were finally washed with PBS, and the coverslips were mounted on glass slides using fluoromount G. Cells were examined with a Zeiss fluorescence microscope equipped with a cooled CCD camera (Spot camera, Qimaging, Surrey, Canada) using an Olympus 1.4 numerical aperture PlanApo ×100 oil immersion objective. All images were processed using the Photoshop software (Adobe Systems Inc.).

TABLE 1

Chemical formulas of polyamine and sequence variability of human α-tubulin

A, chemical formulas of the natural polyamines used in this study. The amino groups are positively charged at physiological pH. *B*, sequence alignment of different human α-tubulin isoforms from amino acid residue 410 to the C terminus. Accession numbers are as follows: α1a NM_006009 (NCBI), α3c NP_005992 (NCBI), α4a NP_005991.1 (NCBI), α6 (GenBank™ EAW58057.1), α8 NP_061816.1 (NCBI). Conserved amino acid residues are boxed. Homologous residues are indicated with a dot. The broken line from residue 418 to 433 indicates helix H12.

A

Putrescine	$NH_2(CH_2)_4NH_2$
Spermine	$NH_2(CH_2)_3NH(CH_2)_4NH(CH_2)_3NH_2$

B

```
                410       420       430       440       450
Alpha 1a  GEGMEEGEFSEAREDMAALEKDYEEVGVDSVEGEGEEEGEEY
Alpha 3c  GEGMEEGEFSEAREDLAALEKDYEEVGVDSVEAEAEE-GEEY
Alpha 4a  GEGMEEGEFSEAREDMAALEKDYEEVGIDSYED--EDEGEE-
Alpha 6   GEGMEEGEFSEAREDMAALEKDYEEVGADSADG--EDEGEEY
Alpha 8   GEGMEEGEFSEAREDLAALEKDYEEVGTDSFE-E-ENEGEEF
```

Preparation of Free and Polymerized Tubulin Fractions from Cultured Cells—The cellular content of free tubulin and microtubules was determined using the method described by Gundersen *et al.* (32) with minor modifications. Cultured HeLa cells were rinsed with 85 mM Pipes, pH 6.9, 1 mM EGTA, 1 mM $MgCl_2$, 2 M glycerol at 37 °C. Extraction of free tubulin was done using the same buffer but containing 0.4% Triton X-100. After 3 min, the extraction buffer containing free tubulin was gently transferred to a graduated tube, mixed with one-quarter volume of 5× SDS-PAGE buffer (325 mM Tris-HCl, pH 6.9, 10% SDS, 30% glycerol, and 1 mM phenylmethylsulfonyl fluoride), and boiled for denaturation. The polymerized tubulin fraction, corresponding to microtubules remaining in the cells, was then solubilized in a volume of 1× SDS buffer equivalent to that used for the soluble fraction and boiled for denaturation. The tubulin content of each fraction was determined by immunoblotting as follows. Proteins were separated by 10% SDS-PAGE and transferred to a PVDF membrane (Invitrogen). The membrane was blocked in 5% nonfat dry milk, PBS for 30 min at room temperature and incubated for 1 h at room temperature with primary E7 anti-tubulin or anti-GFP antibody at 1:15,000 dilution. Bound antibodies were detected with an Odyssey imaging system (LI-COR Biosciences, Lincoln, NE) using anti-mouse-IRDye 800 secondary antibodies (Odyssey, 1:5000 dilution).

RESULTS

Structural Analysis of the αTub410C Peptide—The αTub410C peptide comprises the last 42 C-terminal residues of human α-tubulin (isoform α1a; Table 1*B*). Large amounts of pure and soluble recombinant αTub410C peptide were easily extracted and purified from *E. coli* culture (see supplemental Fig. 1*A*). The two-dimensional ^1H-^{15}N HSQC NMR

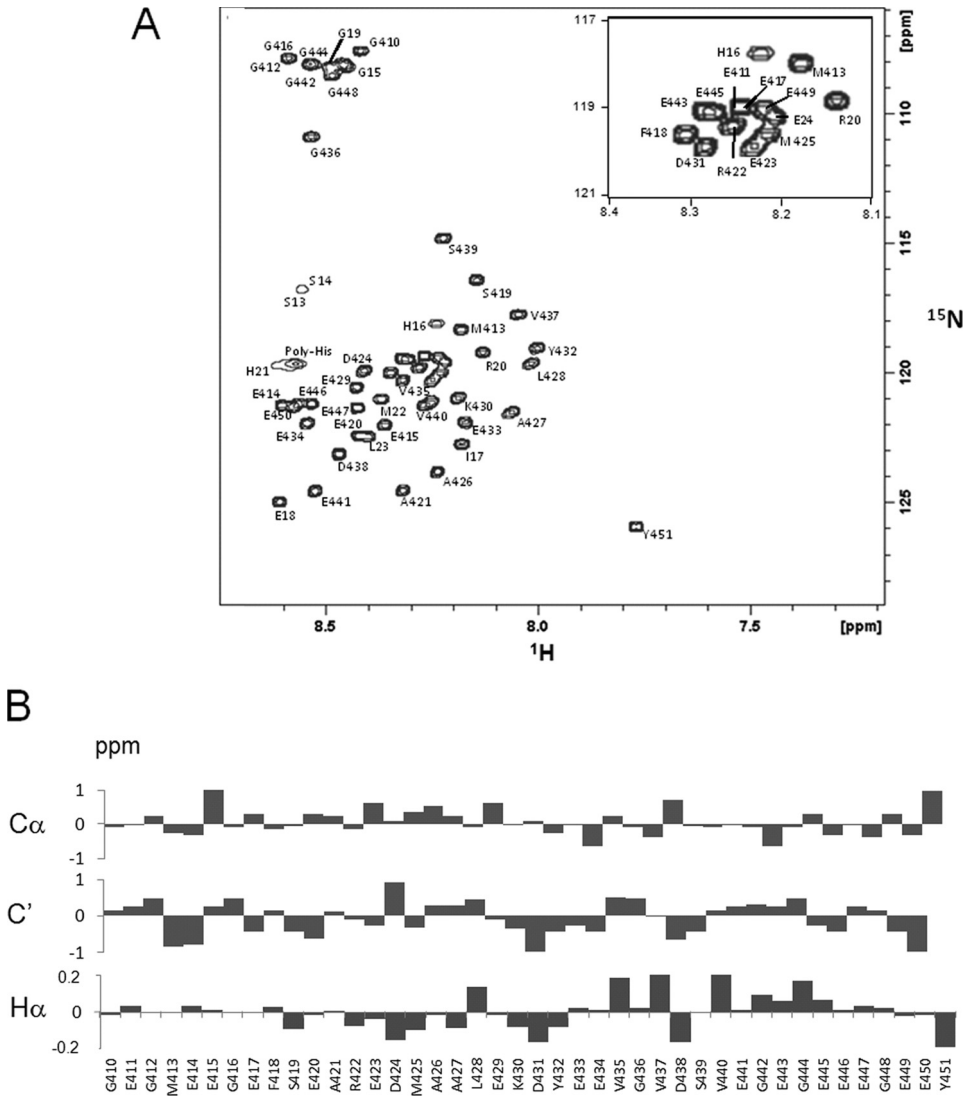

FIGURE 1. **The αTub410C peptide is not structured in aqueous solution.** *A*, assigned ^{1}H-^{15}N HSQC of the αTub410C peptide in 20 mM MES-KOH, pH 6.9, at $T = 20$ °C. All amide protons were assigned. *B*, secondary chemical shifts of the αTub410C peptide in 20 mM MES-KOH, pH 6.9, at $T = 20$ °C. ^{13}Cα, ^{13}C′, and H_α are presented.

spectrum of αTub410C peptide in aqueous buffer shows very well resolved and sharp resonances (Fig. 1*A*), with a low dispersion of the amide region (less than 1 ppm on and about 20 ppm on ^{15}N dimensions). This suggests that, under these conditions, the αTub410C peptide probably does not fold into any tertiary structure, as suggested by previous CD experiments (14). Complete NMR assignment of the backbone resonances of αTub410C was realized (see supplemental Table 1). Chemical shift deviations from random coil values (33) of ^{13}Cα, ^{13}C′, and ^{1}Hα also indicate that no significant secondary structure is present even if the ^{1}Hα chemical shifts suggest a weak helical propensity for amino acid residues 424–432 (Fig. 1*B*).

Binding of Tau to the αTub410C Peptide; Identification of the Binding Region, Stoichiometry, and Thermodynamic Values—Tau is mainly a neuronal MAP of the CNS. Six Tau isoforms can be expressed resulting from the alternative splicing of a single gene. hTau40, used in the present work, which is the longest human isoform, contains four repeats involved in the binding to tubulin/microtubules and two inserts in the N-terminal projection domain. Many studies have shown that the tubulin C-terminal domain is implicated in the Tau-microtubule interaction. Electron microscopy experiments showed that Tau binds longitudinally to the outer ridges of microtubule protofilaments, suggesting that the exposed C-terminal tubulin domain constitutes an important binding site (34). Direct interaction between Tau and the tubulin C-terminal region was also demonstrated but was not characterized at the residue scale (15, 35, 36). In the present work, we used purified Tau (see supplemental Fig. 1*B*) and attempted to describe this aspect using two-dimensional ^{1}H-^{15}N HSQC experiments. As shown in Fig. 2*A*, several resonances of the ^{15}N-labeled αTub410C spectrum were affected by the presence of Tau. Interestingly, the binding of Tau affects a large and continuous stretch of residues on the αTub410C, as reflected by large chemical shift perturbations of residues in the region between amino acid residues 421 and 441 (Fig. 2*B*).

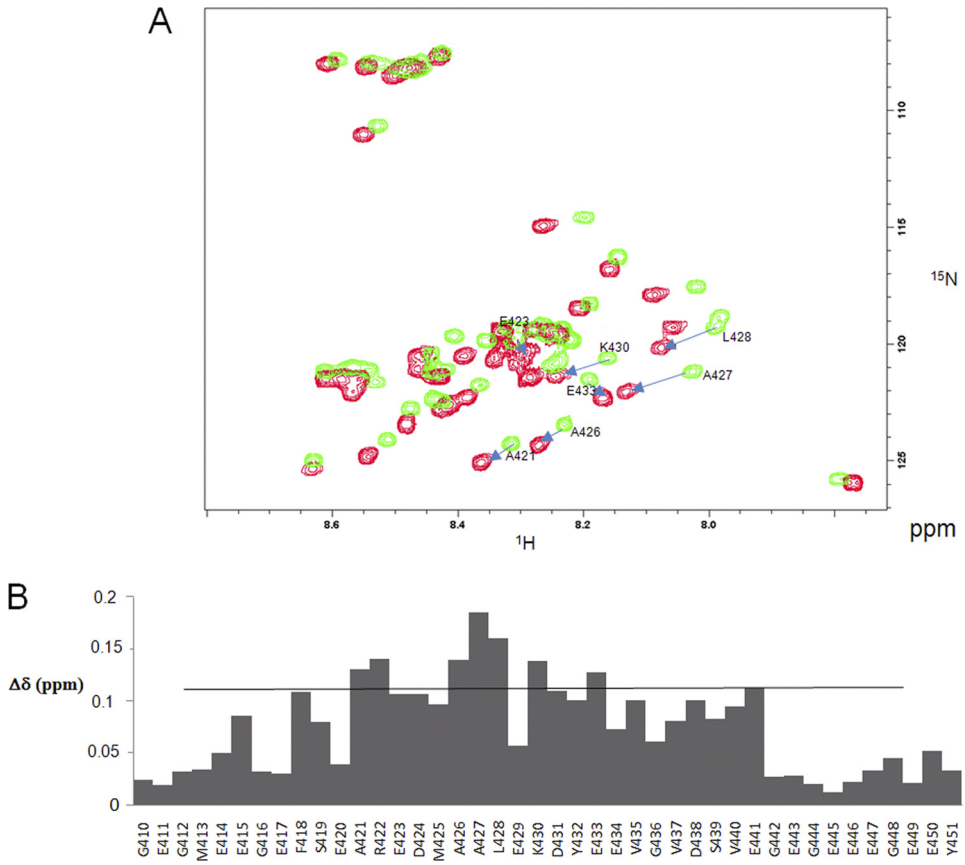

FIGURE 2. **Titration analyses of the interaction between Tau and αTub410C.** *A*, ^{1}H-^{15}N HSQC of 80 μM αTub410C in 20 mM MES-KOH, pH 6.9, 1 mM DTT, at $T = 20$ °C in the absence (*green*) and presence (*red*) of 10 μM Tau. Residues with the greatest chemical shift perturbations are shown. *B*, mapping of the chemical shift perturbations observed in the ^{1}H-^{15}N HSQC Tau-αTub410C titration experiments. The chemical shift perturbation values were calculated as described under "Materials and Methods."

We next carried out ITC experiments to quantify the Tau-αTub410C interaction. Fig. 3*A* displays the isotherms of Tau titration into the αTub410C solution. The best fit of the integrated isotherm using a single-site model indicated that Tau binds to eight αTub410C molecules with a K_d value of 0.4 μM. The high negative value of enthalpy reflects the highly electrostatic interaction and the unfavorable entropic contribution is probably due to the loss of mobility of the eight αTub410C peptides bound to Tau (Fig. 3*B*). Tau possesses two cysteine residues, which can participate in either intra- or intermolecular disulfide bridges (to form in the later case oligomeric forms, such as dimers and trimers). We thus evaluated the influence of the oxidation state of Tau on αTub410C binding using ITC. In similar conditions but in the absence of DTT, no titration could be observed. This result is in agreement with previous work, which showed that the affinity of Tau for microtubules decreases in the absence of DTT using co-sedimentation and NMR titration assays (37, 38).

Binding of Spermine and Putrescine to the αTub410C Peptide; Identification of the Binding Region, Stoichiometry, and Thermodynamic Values—Promotion of microtubule assembly by polyamines requires the presence of the C-terminal tail of tubulin (39, 40). First, we checked that the interaction of putrescine and spermine with full-length αβ-tubulin can be analyzed by NMR. After this positive control, we next focused our investigations on the spermine-αTub410C interaction.

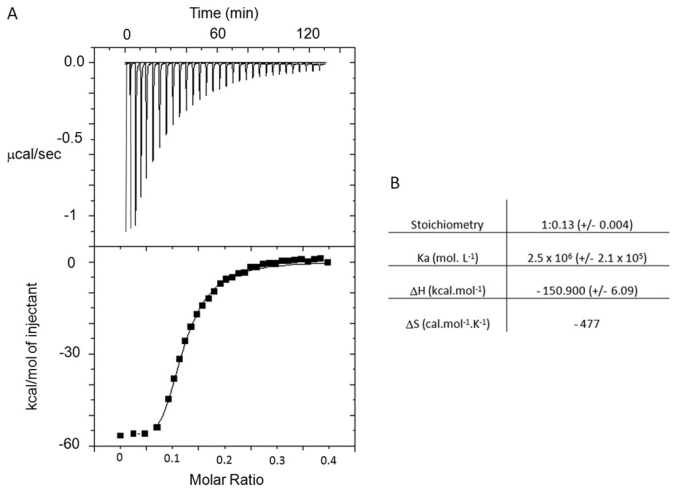

FIGURE 3. **Isothermal titration calorimetric analyses of the interactions between Tau and αTub410C.** *A*, trace of the calorimetric titration of 32 × 5-μl aliquots of hTau40 (22 μM) into the cell containing the αTub410C (8 μM). *Lower panel*, integrated binding isotherm obtained from the experiment. *B*, parameters obtained from the best fit.

The NMR assignment of putrescine and spermine protons was achieved using 1 mM polyamine samples in buffer solution. Spermine proton resonances were observed at 2.85, 1.85, and 1.55 ppm. The 1.55 ppm peak was the most intense and was subsequently used to monitor polyamine-tubulin interaction. As shown in Fig. 4*A*, in the presence of 40 μM full-length

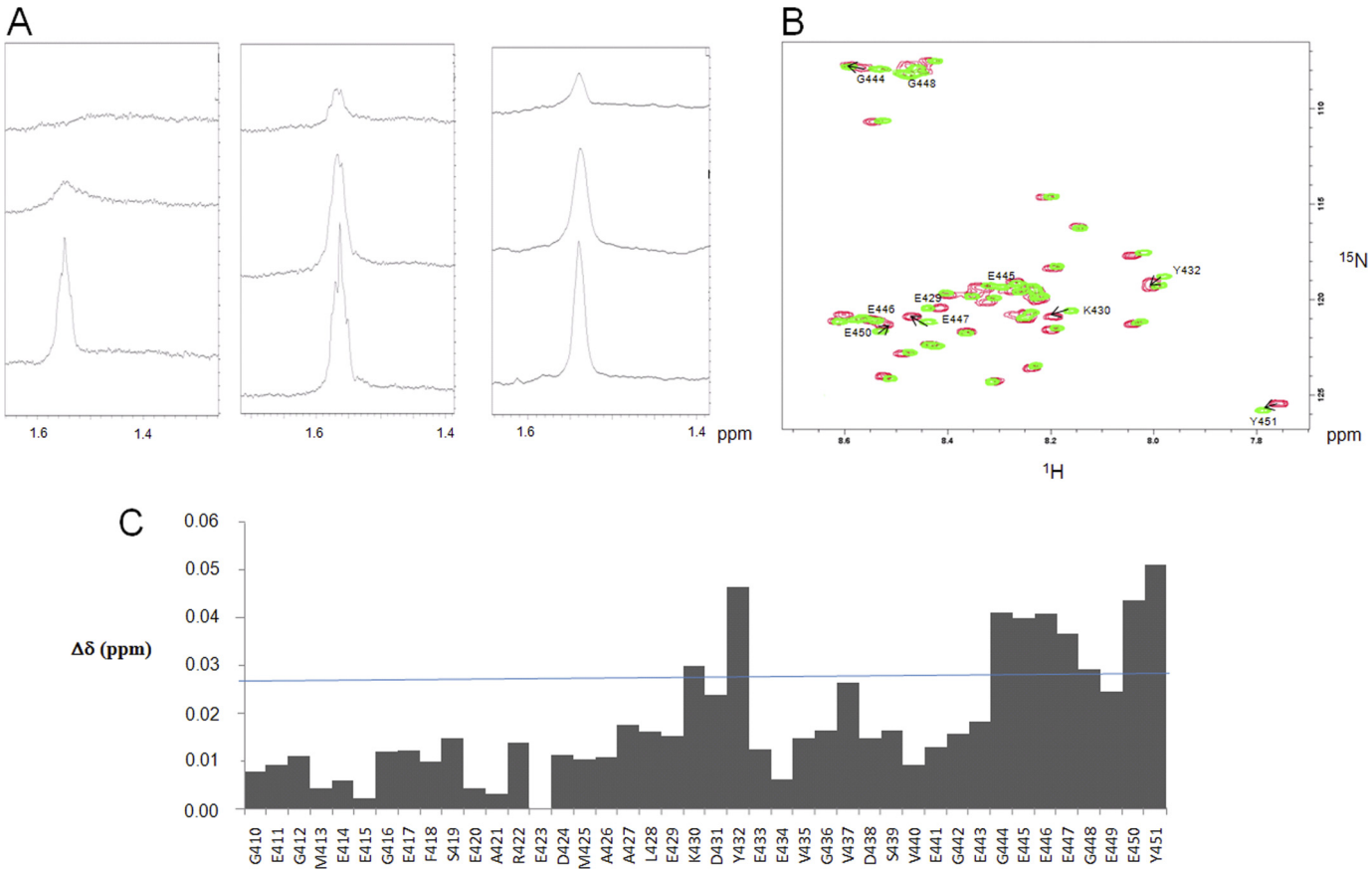

FIGURE 4. **Small polyamines interact with tubulin through electrostatic bonds.** *A*, *left*, one-dimensional ^{1}H NMR spectrum (*zoomed*) in the 1.4–1.6 ppm region obtained with 40 μM tubulin, 20 mM MES-KOH, pH 6.9, 2 mM $MgCl_2$, 20% glycerol at $T = 20$ °C in the presence of 300 μM (*upper spectrum*) or 1 mM (*middle spectrum*) spermine. 500 mM KCl was added at the end of the experiment in the sample to examine the impact of high ionic strength (*lower spectrum*). *Middle*, one-dimensional ^{1}H NMR spectrum (*zoomed*) on the 1.4–1.6 ppm region obtained with 40 μM tubulin, 20 mM MES-KOH, pH 6.9, 2 mM $MgCl_2$, 20% glycerol at $T = 20$ °C in the presence of 300 μM (*upper spectrum*) or 1 mM (*middle spectrum*) putrescine. 500 mM KCl was added at the end of the experiment in the sample to examine the impact of high ionic strength (*lower spectrum*). *Right*, one-dimensional ^{1}H NMR spectrum (*zoomed*) in the 1.4–1.6 ppm region obtained with 40 μM tubulin S, 20 mM MES-KOH, pH 6.9, 2 mM $MgCl_2$, 20% glycerol at $T = 20$ °C in the presence of 300 μM (*upper spectrum*) or 1 mM (*middle spectrum*) spermine. 500 mM KCl was added at the end of the experiment in the sample to examine the impact of high ionic strength (*lower spectrum*). *B*, ^{1}H-^{15}N HSQC spectrum of 200 μM αTub410C in 20 mM MES-KOH, pH 6.9, at $T = 20$ °C in the absence (*green*) and presence (*red*) of 3 mM spermine. The amino acid residues with the most perturbated chemical shifts are indicated. *C*, chemical shift perturbations from the ^{1}H-^{15}N HSQC spectrum observed in the absence and presence of 3 mM spermine. The chemical shift perturbation values were calculated according to the formula, $((\Delta\delta^{1}H)^2 + (\Delta\delta^{15}N)^2/6.5^2)^{1/2}$ (31).

αβ-tubulin, the 1.55 ppm peak of spermine at 300 μM completely disappeared, whereas it remained partly visible with 1 mM. Interestingly, the addition of 500 mM KCl to the 40 μM tubulin and 1 mM spermine sample completely restored the spermine signal in agreement with a dissociation of the complex. This also indicated that the spermine-tubulin interaction is mostly electrostatic. When such experiments were performed with putrescine, which presents only two positive charges, the 1.55 ppm peak remained partly visible at 300 μM and was almost at full intensity at 1 mM. Again, the maximum signal was recovered in the presence of KCl. These results show that spermine interacts more tightly than putrescine with tubulin. To provide further information regarding the polyamine binding site on tubulin, similar experiments were carried out using tubulin S, which showed no spermine binding (Fig. 4*A*). This latter result strengthens the proposal that polyamines interfere with microtubule dynamics mainly through interaction with the C-terminal domain of tubulin.

The interaction between spermine and the αTub410C peptide was then examined in detail using two-dimensional ^{1}H-^{15}N HSQC experiments. Titration experiments based on chemical shift perturbation of the αTub410C resonances were performed with increasing concentrations of spermine. The superimposition of the 200 μM αTub410C peptide spectra in the absence and presence of 3 mM spermine is shown in Fig. 4*B*. No broadened or new resonances appeared in the presence of spermine, but we observed that several resonances were shifted. Mean weight chemical shift displacements are displayed in Fig. 4*C*, which shows that two regions of the αTub410C peptide are influenced by the interaction with spermine: amino acid residues 430–432 and 444–451. We found again here that in the presence of 3 mM spermine and 500 mM KCl, the resonances observed on the HSQC spectrum of αTub410C were not shifted compared with those of the HSQC spectrum obtained with the αTub410C peptide alone (data not shown). This is in agreement with an abolition of the binding of spermine to the αTub410C peptide by a high concentration of KCl, which also suggests that polar interactions are involved in this binding. The spermine-αTub410C interaction was also examined using NOESY ^{1}H-^{15}N HSQC

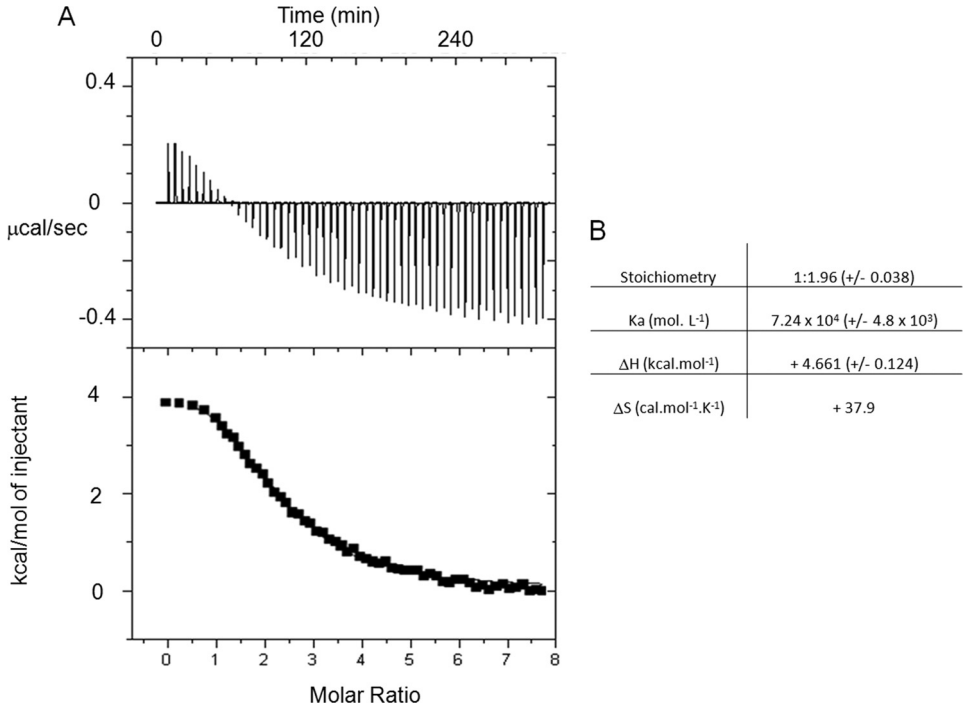

FIGURE 5. **Isothermal titration calorimetric analyses of the interactions between spermine and αTub410C.** *A*, trace of the calorimetric titration of 55 aliquots (10-µl) of spermine (1.5 mM) into the cell containing αTub410C (11 µM). *Lower panel*, integrated binding isotherm obtained from the experiment. *B*, parameters obtained from the best fit.

experiments, which showed some intermolecular NOEs (see supplemental Fig. 1*C*). We then performed similar titration experiments with putrescine up to a concentration of 10 mM. No significant chemical shift changes were detected during titration, suggesting that the putrescine binding to αTub410C is too weak to be detected by NMR (the superimposition of the two spectra is displayed in supplemental Fig. 2). As a control, the αTub410C peptide was titrated with NH_4Cl (up to 20 mM), used as a model monoamine; no significant perturbation was observed. Finally, the binding of spermine to αTub410C was quantified by ITC experiments. Fig. 5*A* shows the calorimetric trace of a typical experiment of spermine injection into an αTub410C solution. The best fit of the integrated isotherm using a single-site model indicates that two spermine molecules bind to one αTub410C peptide with a K_d value of 14 µM (Fig. 5*B*). Similar experiments were realized to characterize the putrescine-αTub410C interaction, and the results showed a very high K_d (data not shown).

The present results show that Tau and spermine interact with the αTub410C peptide and that their binding regions on αTub410C share some common residues (Lys^{430}, Asp^{431}, and Tyr^{432}). We thus examined the possibility of a Tau/spermine competition for αTub410C binding using two-dimensional ^1H-^{15}N HSQC titration experiments. αTub410C (100 µM) was incubated in the presence of 40 µM Tau, and then spermine was added. The results show that the ^1H-^{15}N HSQC spectrum progressively shifted from the aspect of the Tau·αTub410C complex to that of the spermine·αTub410C complex, suggesting that the excess of spermine releases Tau from αTub410C. At 9 mM spermine, we finally obtained the spectrum characteristic of the spermine·αTub410C complex (Fig. 6*A*). In order to make sure that those high concentra-

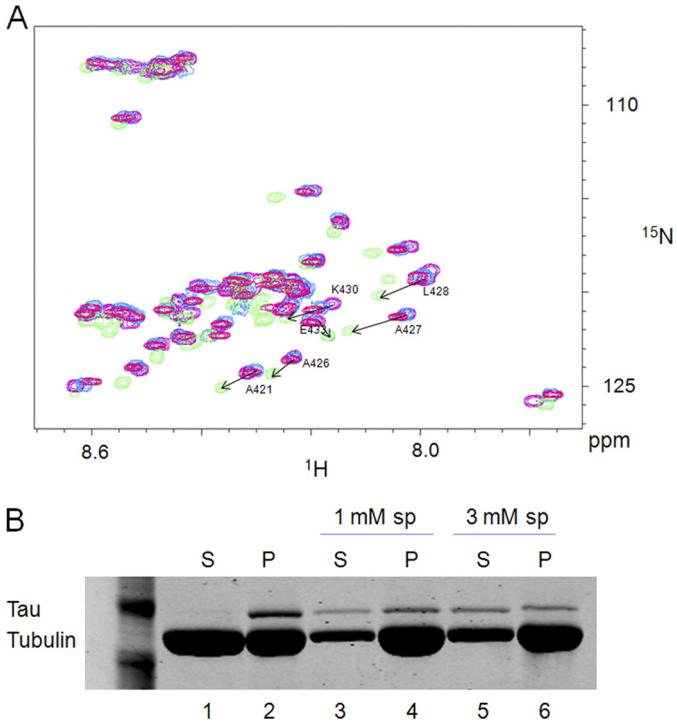

FIGURE 6. **Tau and spermine compete for binding to the αTub410C peptide.** *A*, ^1H-^{15}N HSQC spectrum of 100 µM αTub410C in 20 mM MES-KOH, pH 6.9, 1 mM DTT at $T = 20$ °C in the absence (*purple*) or presence of 40 µM Tau (*green*) with spermine alone (9 mM) (*pink*) and with both 40 µM Tau and 9 mM spermine (*blue*). *B*, 40 µM tubulin was polymerized at 37 °C in 40 mM MES-KOH, pH 6.9, 1 mM GTP, 1 mM DTT, 4 mM $MgCl_2$ in the presence of 50 µM Tau. After centrifugation (25,000 × *g*, 15 min at 37 °C), the pellet was resuspended and depolymerized at 4 °C for 10 min and separated into three aliquots (without spermine, with 1 mM spermine (*sp*), or with 3 mM spermine) and then placed at 37 °C for 15 min. After a second centrifugation (25,000 × *g*, 15 min at 37 °C), supernatants (*S*) and pellets (*P*) were analyzed by 12% SDS-PAGE.

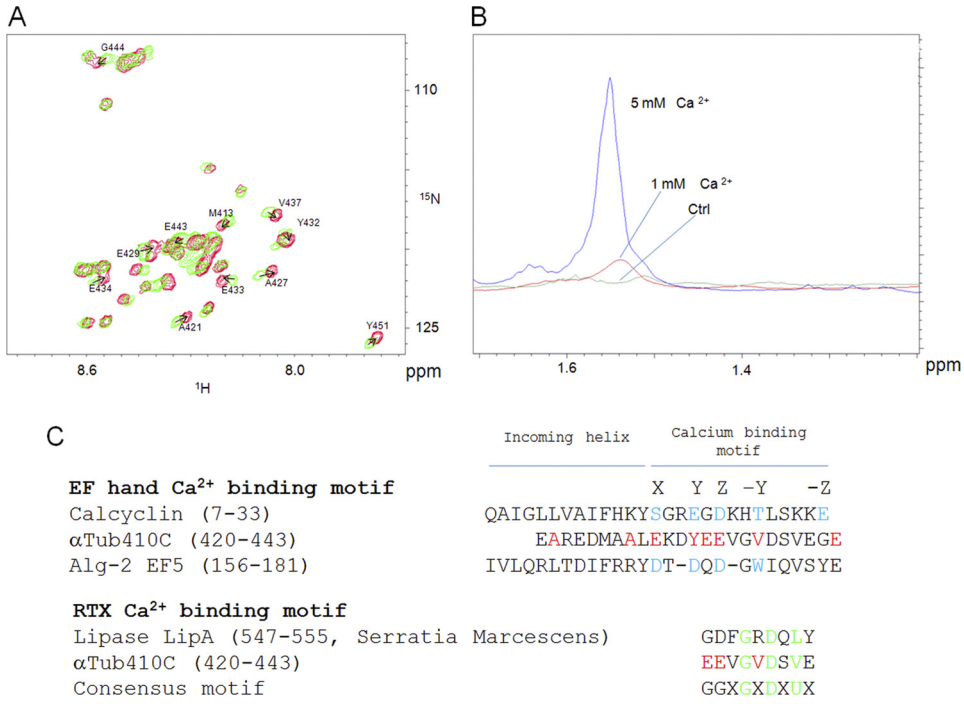

FIGURE 7. **Ca^{2+} interacts with a 23 amino acid region of the αTub410C peptide and competes for spermine binding.** *A*, ^{1}H-^{15}N HSQC spectrum of 200 μM αTub410C in 20 mM MES-KOH, pH 6.9, at $T = 20$ °C in the absence (*green*) and presence of 6 mM calcium (*red*). The residues with the most perturbed chemical shifts are indicated with *arrows*. *B*, one-dimensional ^{1}H NMR spectrum (*zoomed*) on the 1.4–1.65 ppm region obtained with 20 mM MES-KOH, pH 6.9, 2 mM $MgCl_2$, 20% glycerol, 40 μM tubulin at $T = 20$ °C in the presence of 300 μM spermine (*green*). Calcium was added up to 1 mM (*red*) and 5 mM (*blue*). *C*, alignment of two EF-hand sequences with the αTub410C peptide. *X*, *Y*, *Z*, −*Y*, and −*Z* indicate the coordinating positions. The −*Y* Ca^{2+} position is always the main chain carbonyl oxygen. *Red* (for αTub410C), chemical shift perturbation greater than 0.03 ppm. *Blue*, coordinating positions. Sequence alignment of a RT*X* calcium binding motif with the αTub410C peptide. The residues that are particularly conserved are *colored* in *green*. In the consensus motif, *U* corresponds to a hydrophobic residue.

tions of spermine do not cause the aggregation of Tau, which may explain the loss of its binding to αTub410C, the sample was centrifuged and analyzed by SDS-PAGE. The result showed that Tau remains in the soluble fraction in these conditions (see supplemental Fig. 3*A*).

The possibility of a Tau/spermine competition for αTub410C binding was thereafter tested by co-sedimentation experiments as a second investigation method using microtubules. In the absence of spermine, Tau was found almost exclusively associated with microtubules, in good agreement with previous reports (Fig. 6*B*, *lanes 1* and *2*) (37, 41). In the presence of spermine, we first observed an increase of the microtubule mass due to the positive effect of polyamines on microtubule assembly (40). In addition, a fraction of Tau was displaced by spermine and found in the supernatant (compare *lanes 1*, *3*, and *5*). These results indicate that the Tau/spermine competition observed with the isolated αTub410C peptide reflects, at least in part, the more complex Tau-microtubule interaction.

Interaction of Calcium with αTub410C; Identification of the Binding Region—Calcium has been demonstrated to have a high affinity binding site on the C-terminal region of both tubulin subunits (25). However, to date, the precise location of this site remains unknown. We first attempted to define the calcium binding region on the αTub410C peptide using the chemical shift perturbation method based on two-dimensional ^{1}H-^{15}N HSQC titration experiments. Compared with the 200 μM αTub410C control spectrum, the presence of calcium was responsible for a series of significant chemical shift changes of the resonances of the αTub410C peptide, which were maximal for a calcium concentration of 6 mM (Fig. 7*A*). The main differences (except for the C-terminal residue) concerned four glutamates (Glu^{429}, Glu^{433}, Glu^{434}, and Glu^{443}) and four hydrophobic residues (Ala^{421}, Ala^{427}, Tyr^{432}, and Val^{437}). The chemical shift perturbation reflects local folding modifications or charge effects and helped us to delimitate the high affinity calcium binding region (from amino acid residue 421 to 443). Because the binding regions of calcium and spermine overlap (amino acid residues 430–432), we probed the possibility of a competition for αTub410C binding. As shown above, in the presence of 40 μM tubulin, the 1.55 ppm ^{1}H resonance peak of 300 μM spermine disappeared completely. Interestingly, we observed that this spermine peak reappeared progressively with the addition of calcium, and a plateau value was reached for a final calcium concentration of 5 mM (Fig. 7*B*). Similar competition experiments were realized using magnesium, an alternative divalent cation. The results show that magnesium, up to 5 mM, is unable to displace spermine from tubulin, suggesting that the calcium/spermine competition is specific (see supplemental Fig. 3*B*). To probe the impact of such competitions on full-length tubulin assembly in more physiological conditions, we examined whether the inhibition of microtubule assembly by calcium could be reversed by either spermine or Tau and *vice versa*. We observed that 350 μM spermine was sufficient to mask the inhibition of microtubule assembly due to 50 μM

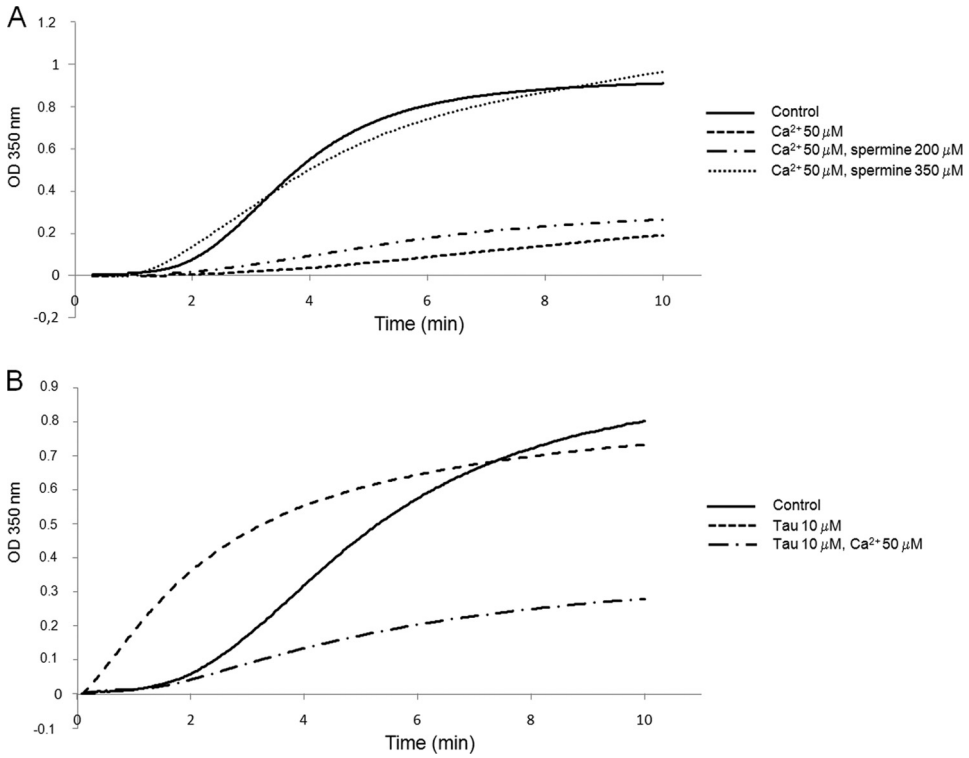

FIGURE 8. **Calcium opposes the promotion of microtubule assembly by tubulin cationic partners.** 30 μM tubulin polymerization was monitored turbidimetrically at 350 nm at 37 °C in 20 mM MES-KOH, pH 6.9, 2 mM $MgCl_2$, and 1 mM GTP with 25% glycerol (*panels A* and *B*). Tau, spermine, and calcium were added at the concentrations indicated in the figure.

calcium (Fig. 8*A*) and that 50 μM calcium inhibits the microtubule promotion effect of 10 μM Tau (Fig. 8*B*).

The Last 23 Residues of α-Tubulin Contribute to the Insertion of Tubulin into Microtubules—We demonstrated here that some residues from an α-tubulin tail peptide are targeted by Tau (residues 421–441), spermine (residues 430–432 and 444–451), and calcium (residues 421–443). In order to examine the contribution of the 429–451 region in living cells, we transfected HeLa cells with a truncated form of α-tubulin, which was deleted from the last 23 residues (GFP-TubΔ23C). We evaluated the ability of this recombinant protein to incorporate into microtubules. Because it was noted that GFP could impede the insertion of β-tubulin into microtubules (42), we first checked, as a control, that a GFP-Tub fusion protein could incorporate in the microtubule network (Fig. 9, *A* and *B* (*top*), *C* and supplemental Fig. 4). When cells were transfected with the GFP-TubΔ23C construct, we observed, in contrast to full-length tubulin, that the truncated protein was not able to incorporate significantly into microtubules but appeared mainly diffused in the cytosol (Fig. 9, *A* and *B* (*bottom*), *C*, and supplemental Fig. 4). Transfection with GFP-TubΔ13C plasmid showed that this protein was unable to incorporate into microtubules. In contrast, in the presence of taxol, GFP-TubΔ13C could be incorporated normally in the microtubule network (Fig. 9*A* and *B* (*middle*) and supplemental Fig. 4).

DISCUSSION

Structure and Functionality of the αTub410C Peptide—The atomic structures currently available for the full-length tubulin (zinc sheets or tubulin·RB3-stathmin-like domain complexes) show the presence of an α-helix over amino acid residues 418–433 but provide no information on the very last charged tails of α- and β-tubulin. This lack of structural data reflects the disordered character of this region of tubulin and justifies molecular modeling efforts as a tool for a better understanding of its function. Molecular modeling actually predicts significant variations of the interaction of this region with MAPs as the sequence varies (43). There is, however, a need to document experimentally the structure-function relationships of the C-terminal domain of tubulin because it is involved in key regulation processes for microtubule assembly. One possibility to overcome these difficulties is to consider the structure of isolated tubulin C-terminal peptides and to study their behaviors in the presence of binding partners. The present NMR solution structure investigation on the αTub410C peptide, which comprises the acidic tail of α-tubulin, confirms that this segment is mainly disordered when free in aqueous solution (Fig. 1*B*). The absence of a definite fold for this peptide agrees with the fact that it can interact with many different partners (MAPs (15), dynein and kinesin (44), spastin (45), and polycations (25)), a global flexibility being commonly observed in peptides or protein domains that interact with multiple partners because this requires conformational space research (43, 46).

Interaction of Tau with the αTub410C Peptide—We first showed here by NMR and ITC experiments a direct interaction between hTau40 and the αTub410C peptide and measured a K_d value of 0.4 μM. The value of the dissociation con-

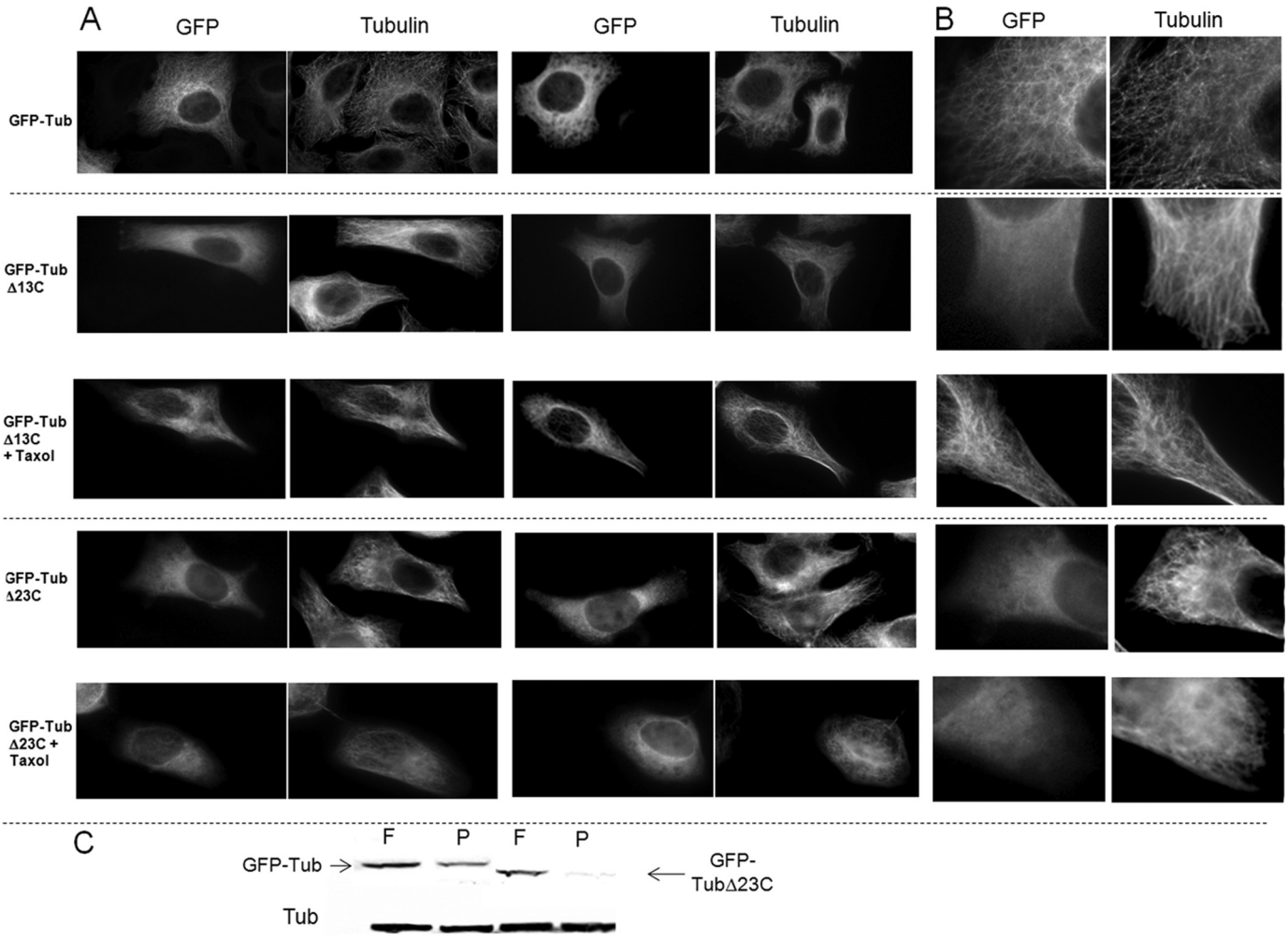

FIGURE 9. **The 23 C-terminal residues of α-tubulin are required for its incorporation into microtubules *in vivo*.** *A*, human GFP-α-tubulin, GFP-α-tubulinΔ13C, and GFP-α-tubulinΔ23C were transfected in HeLa cells (×60 magnification). 24 h post-transfection, 0.5 μM taxol was added for 1 h when indicated in the figure. Cells were fixed and labeled with anti-tubulin antibodies. *B*, higher magnification of previous images. *C*, free (*F*) and polymerized tubulin (*P*) were extracted according to the protocol of Gundersen *et al.* (32). The wild type and recombinant tubulin content of each fraction was determined by Western blotting with anti-tubulin and anti-GFP antibodies, respectively.

stant strongly suggests that the αTub410C peptide represents a critical part of the major binding site for Tau on microtubules because it is close to K_d values measured with full-length tubulin. Indeed, according to Ackmann *et al.* (47), the binding of Tau to microtubules occurs in two structurally and kinetically distinct steps, which comprise a first binding phase with low stoichiometry (0.2–0.3 Tau per tubulin heterodimer) but with a tight binding (K_d ~0.05–0.5 μM) and a second phase of weaker affinity (K_d = 50 μM) but having a higher and nonsaturable stoichiometry. The nonsaturable part of the binding reflects the possibility of a Tau-Tau aggregation at the surface of microtubules. Similarly, Sillen *et al.* (37) found a K_d value of 1.6 μM based on Tau-microtubule co-sedimentation experiments and a K_d of 20 nM when measured by FRET. Differences were attributed to the fact that co-sedimentation does not distinguish Tau-microtubule interaction for more complex $(Tau{\cdot}Tau)_n{\cdot}$microtubule forms, whereas FRET only addresses the direct Tau-microtubule interaction.

There is little information concerning the Tau binding site on tubulin. The present NMR results (Fig. 2) show that upon

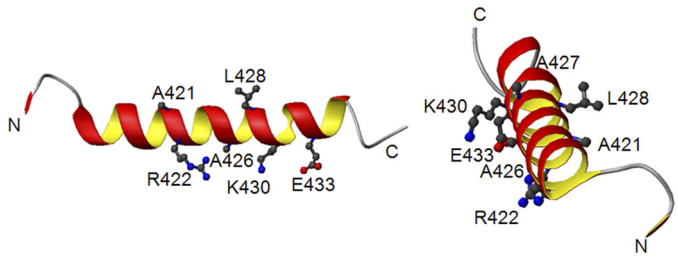

FIGURE 10. **Tau interacts with hydrophobic and charged residues of the αTub410C peptide.** Shown are two representations of a part of the crystallographic structure (fragment 410–439 of α-tubulin) (Protein Data Bank code 1JFF). The side chains of residues that present the greatest perturbations in the presence of Tau are represented. Nitrogens of side chains are *colored* in *blue*, oxygens in *red*, and carbons in *gray*.

Tau binding to the αTub410C peptide, the most perturbed αTub410C chemical shifts concern amino acid residues Ala^{421}, Arg^{422}, Ala^{426}, Ala^{427}, Leu^{428}, Lys^{430}, Glu^{433}, and Glu^{441}, which confirms the role of helix H12. These amino acid residues (except Glu^{441}) are highlighted in Fig. 10 on the tubulin crystal structure (amino acid residues 410–439) (48). These experimental results are in agreement with former

docking data based on cryo-EM experiments, which proposed that Tau lies in close proximity to the end of helix H12 and to the tubulin tail (34). Interestingly, hydrophobic highlighted residues are located on one side of the helix which is in interaction with the core of tubulin. Hydrophilic residues are on the other side, exposed to solvent. The cognate tubulin-binding residues on Tau have been recently mapped by ^{1}H-^{15}N HSQC NMR experiments on taxol-stabilized microtubules. The regions of Tau in strong interaction with tubulin are mainly ^{225}KVAVVRT^{231} in domain P2, ^{245}TAPVPMPDL^{253} in the microtubule binding repeat R1, ^{275}VQIINKKLDLSNV^{287} in R2, ^{306}VQIVYKPVDLSKV^{318} in R3, and 370–380 in R′, whereas residues from R4 did not contribute significantly to microtubule binding (49, 50). In agreement with Mukrasch *et al.* (49), we can also propose that the Tau-αTub410C interaction is partly electrostatic (Lys and Arg of Tau could be located near Glu of αTub410C) and partly hydrophobic (Ala, Val, and Pro of Tau could be located near Ala and Leu of αTub410C). Finally, we measured here a 0.25 Tau/2 αTub410C stoichiometry, a value close but not similar to the 0.48 Tau/tubulin heterodimer value obtained by Sillen *et al.* (37) using FRET experiments. The difference could be due to the fact that the αTub410C peptide is more flexible when free than the corresponding region in microtubules.

Interaction between Polyamines and the αTub410C Peptide—We found here that spermine interacts with the αTub410C peptide with a 2:1 spermine/αTub410C stoichiometry on two separated binding regions (Fig. 4*C*). The ITC titration data show a single transition upon spermine binding to αTub410C, suggesting that the two spermine binding sites have comparable K_d values. NMR results further indicate that this interaction depends on electrostatic interactions because the spermine·αTub410C peptide complex is fully dissociated at high monovalent salt concentration (500 mM KCl). Interestingly, the spermine-αTub410C interaction is reminiscent of the spermine-α-synuclein interaction because α-synuclein bears nine negative charges concentrated in its last 20 amino acid residues (51). This again underlines the multifunctional character of polyamines.

The concentration of spermine in living cells is very high and can reach the millimolar range within the cytoplasm. Spermine has also long been proposed to be mainly in complex with nucleic acids (DNA and RNA) (for a review, see Ref. 52). Interestingly, the 14 μM dissociation constant measured here for the spermine-αTub410C interaction is not far from that of the spermine-DNA interaction (53, 54) or for spermine-$GIRK_{CP}$ potassium channel interaction (55). This indeed is most probably related to the simple structure of spermine, but importantly, this strongly suggests that a significant amount of spermine may be available to interact with microtubules that represent a considerable surface within the cell. The spermine-microtubule interaction could hence be relevant for the regulation of microtubule dynamics *in vivo* by two different mechanisms: (i) a direct binding to microtubule or (ii) the possibility to displace MAPs from microtubule binding (21). This latter possibility is strengthened by the observation that a high concentration of polyamines can still enhance tubulin polymerization in the presence of MAPs (20, 40). We also found that Tau and spermine have overlapping binding sites on the αTub410C peptide and that the K_d values for both are in the micromolar range. Finally, we showed that Tau and spermine can compete for αTub410C binding by NMR experiments, and the co-sedimentation assays show that this result can be extrapolated to microtubules (Fig. 6*B*).

Interaction of Calcium with the αTub410C Peptide—Calcium is known to inhibit tubulin polymerization either directly or through Ca^{2+}-calmodulin regulation. MAPs could regulate the activation of calmodulin, which has an impact on microtubule disassembly (23, 56, 57). However, the mechanism by which calcium acts directly on tubulin/microtubules still remains unknown. The interaction of Ca^{2+} with the C-terminal part of tubulin was suggested by the fact that the direct inhibition of tubulin assembly by Ca^{2+} disappears when using subtilisin-treated tubulin. A direct binding of Ca^{2+} on proteolytic fragments of the α- or β-tubulin tails was also demonstrated (45, 58), and a high affinity Ca^{2+} binding site was finally proposed in the 423–446 region of the tubulin tail with a K_d evaluated to be 11 μM (59).

In the present work, we localize the calcium binding region on the αTub410C peptide. The greatest NMR chemical shift perturbations were observed for amino acid residues Glu^{429}, Tyr^{432}, Glu^{434}, and Val^{437}, which could participate to the coordination of calcium through a definite fold. The comparison of the αTub410C peptide sequence with different calcium binding domains indeed shows homologies with two calcium binding motifs. The first belongs to the EF-hand family (Fig. 7*C*) (for a review, see Ref. 60), where calcium coordination (in the case of calcyclin) is due to five canonical locations. However, it has been shown for EF5 of ALG-2 that the coordination could be due to only four canonical locations (Fig. 7*C*, amino acid residues *colored blue* (61)). In this case, the linker between the two helices is longer, and the second helix does not participate in the coordination. Because the tubulin tail does not have this second helix, EF5 could be a better model for calcium coordination. The chemical shift perturbations observed here for amino acid residues Glu^{443}, Ala^{421}, and Met^{413} of the αTub410C peptide could hence be due to structural rearrangements. A second hypothesis could be that the αTub410C peptide calcium-binding site is related to the RTX motif. This motif has been shown to be intrinsically disordered in the absence of calcium and to adopt secondary and tertiary structures upon calcium fixation (62). Interestingly, the zone of the greatest chemical shift perturbations observed on the αTub410C peptide upon calcium binding are within the RTX consensus (Fig. 7*C*) (63). This may indicate that the C terminus of tubulin behaves truly as a calcium consensus region. However, despite this information, an NMR structure analysis of the αTub410C peptide in interaction with calcium using Cα, C′, and Hα secondary chemical shifts did not show any secondary and tertiary structural rearrangement (data not shown). Further investigations with longer peptide may solve this apparent contradiction.

Calcium Competes with Tubulin Cationic Partners; Interest for Microtubule Dynamics—It has been demonstrated that calcium causes a concentration-dependent destabilization of microtubules in the presence or absence of MAPs (22, 64). It

was also proposed for a long time that calcium interferes directly with microtubule assembly. We show here that calcium is able to compete with Tau and spermine, two representative members of tubulin cationic partners, for tubulin binding. This suggests that calcium may actually regulate negatively microtubule assembly *in vivo*, either via direct interaction with naked microtubules through a still unknown molecular mechanism or via the displacement of tubulin cationic partners.

Delimitation of Cationic Interaction Zone Related to Post-translational Modifications—We have delimited overlapping amino acid stretches on the α C-terminal region interacting with cationic partners: amino acids 421–441 for Tau, 430–432 and 444–451 for spermine, and 421–443 for calcium. Studies have shown that the polyglutamate chain (on Glu^{445}) does not appear to interact directly with Tau (65). Our data confirm this result. However, it has been shown that polyglutamylation modifies the affinity of Tau for microtubules, probably by a conformational shift in the C-terminal structure (66). Furthermore, with our data, we can propose that polyglutamylation should affect the affinity and the stoichiometry of spermine for tubulin.

The C Terminus of α-Tubulin Is Necessary for Microtubule Incorporation—It was recently shown that the deletion of the charged C-terminal tail of β-tubulin impedes its incorporation in the microtubule network *in vivo* (42). The present results show that this is also the case with α-tubulin truncated of its 23 last residues (GFP-TubΔ23C). Indirect or direct mechanisms could explain these observations as follows: On the one hand, the C-terminal part of tubulin constitutes an important binding site for different partners (proteins, MAPs, and small cationic molecules) implicated in microtubule dynamics. For example, the loss of spermine interaction could slow tubulin diffusion (40). A recent study demonstrated that polyamines influence microtubule network *in vivo* (21). On the other hand, the deletion of the last 23 amino acid residues could have a structural impact on the globular part of the tubulin implicated in microtubule assembly. This hypothesis is strengthened by the fact that some conserved amino acid residues that belong to the helix H12 (418–433) are missing in the GFP-TubΔ23C mutant. In order to observe the impact of the truncation of helix H12, we compared microtubule incorporation of the GFP-TubΔ23C mutant with the GFP-TubΔ13C mutant (which contains the full helix H12). Results showed that this mutant is also unable to incorporate in the microtubule network, suggesting that the unique absence of H12 is not the direct cause for the nonincorporation of the GFP-TubΔ23C. However, the two mutants show different results in the presence of taxol, which decreases tubulin critical concentration. Although incorporation remains impossible for GFP-TubΔ23C in the presence of taxol, the incorporation of GFP-TubΔ13C becomes comparable with the control GFP-Tub. This result shows that tubulin is still functional after the deletion of the last 13 C-terminal amino acid residues and that the indirect effect could be the better hypothesis for this mutant. Concerning the GFP-TubΔ23C mutant, the nonincorporation could be due to a structural effect. It can be emphasized that the loss of post-translational modifications on the deleted C-terminal mutants provides more complexity to the interpretation of these results. Further experiments are required to elucidate the precise role of these amino acid residues *in vivo*.

In conclusion, the results provide a detailed description of the binding regions of Tau, spermine, and calcium on the α-tubulin C-terminal end. We demonstrated in cells that this region of tubulin is critical for microtubule assembly and that *in vitro* calcium is able to compete with the fixation of tubulin cationic partners. Further experiments should demonstrate whether such a direct competition can participate in the regulation of microtubule dynamics in cells, particularly in relation to cell signaling.

Acknowledgments—We thank Sylviane Hoos and Patrick England from the Center of Biophysic of Macromolecules and Their Interactions (Institut Pasteur, Paris, France) for help, technical support, and fruitful discussions.

REFERENCES

1. Ponstingl, H., Little, M., Krauhs, E., and Kempf, T. (1979) *Nature* **282,** 423–425
2. Ponstingl, H., Krauhs, E., Little, M., and Kempf, T. (1981) *Proc. Natl. Acad. Sci. U.S.A.* **78,** 2757–2761
3. Krauhs, E., Little, M., Kempf, T., Hofer-Warbinek, R., Ade, W., and Ponstingl, H. (1981) *Proc. Natl. Acad. Sci. U.S.A.* **78,** 4156–4160
4. Ponstingl, H., Krauhs, E., Little, M., Kempf, T., Hofer-Warbinek, R., and Ade, W. (1982) *Cold Spring Harb. Symp. Quant. Biol.* **46,** 191–197
5. Nogales, E., Wolf, S. G., and Downing, K. H. (1998) *Nature* **391,** 199–203
6. Serrano, L., de la Torre, J., Maccioni, R. B., and Avila, J. (1984) *Proc. Natl. Acad. Sci. U.S.A.* **81,** 5989–5993
7. Maccioni, R. B., Serrano, L., Avila, J., and Cann, J. R. (1986) *Eur. J. Biochem.* **156,** 375–381
8. Serrano, L., Avila, J., and Maccioni, R. B. (1984) *Biochemistry* **23,** 4675–4681
9. Kuznetsov, S. A., Gelfand, V. I., Rodionov, V. I., Rosenblat, V. A., and Gulyaeva, J. G. (1978) *FEBS Lett.* **95,** 343–346
10. Little, M., and Seehaus, T. (1988) *Comp. Biochem. Physiol. B* **90,** 655–670
11. Ravelli, R. B., Gigant, B., Curmi, P. A., Jourdain, I., Lachkar, S., Sobel, A., and Knossow, M. (2004) *Nature* **428,** 198–202
12. Gigant, B., Curmi, P. A., Martin-Barbey, C., Charbaut, E., Lachkar, S., Lebeau, L., Siavoshian, S., Sobel, A., and Knossow, M. (2000) *Cell* **102,** 809–816
13. Gigant, B., Wang, C., Ravelli, R. B., Roussi, F., Steinmetz, M. O., Curmi, P. A., Sobel, A., and Knossow, M. (2005) *Nature* **435,** 519–522
14. Jimenez, M. A., Evangelio, J. A., Aranda, C., Lopez-Brauet, A., Andreu, D., Rico, M., Lagos, R., Andreu, J. M., and Monasterio, O. (1999) *Protein Sci.* **8,** 788–799
15. Littauer, U. Z., Giveon, D., Thierauf, M., Ginzburg, I., and Ponstingl, H. (1986) *Proc. Natl. Acad. Sci. U.S.A.* **83,** 7162–7166
16. Maccioni, R. B., Rivas, C. I., and Vera, J. C. (1988) *EMBO J.* **7,** 1957–1963
17. Maccioni, R. B., and Cambiazo, V. (1995) *Physiol. Rev.* **75,** 835–864
18. Hirokawa, N. (1994) *Curr. Opin. Cell Biol.* **6,** 74–81
19. Mishima, M., Maesaki, R., Kasa, M., Watanabe, T., Fukata, M., Kaibuchi, K., and Hakoshima, T. (2007) *Proc. Natl. Acad. Sci. U.S.A.* **104,** 10346–10351
20. Anderson, P. J., Bardocz, S., Campos, R., and Brown, D. L. (1985) *Biochem. Biophys. Res. Commun.* **132,** 147–154
21. Savarin, P., Barbet, A., Delga, S., Joshi, V., Hamon, L., Lefevre, J., Nakib, S., De Bandt, J. P., Moinard, C., Curmi, P. A., and Pastré, D. (2010) *Biochem. J.* **430,** 151–159
22. Strömberg, E., and Wallin, M. (1994) *Cell Motil. Cytoskeleton* **28,** 59–68

23. Weisenberg, R. C. (1972) *Science* **177,** 1104–1105
24. Solomon, F. (1977) *Biochemistry* **16,** 358–363
25. Serrano, L., Valencia, A., Caballero, R., and Avila, J. (1986) *J. Biol. Chem.* **261,** 7076–7081
26. Castoldi, M., and Popov, A. V. (2003) *Protein Expr. Purif.* **32,** 83–88
27. Knipling, L., Hwang, J., and Wolff, J. (1999) *Cell Motil. Cytoskeleton* **43,** 63–71
28. Detrich, H. W., 3rd, and Williams, R. C. (1978) *Biochemistry* **17,** 3900–3917
29. Grzesiek, S., and Bax, A. (1993) *J. Biomol. NMR* **3,** 185–204
30. Johnson, B. A., and Blevins, R. A. (1994) *J. Biomol. NMR* **4,** 603–614
31. Mulder, F. A., Schipper, D., Bott, R., and Boelens, R. (1999) *J. Mol. Biol.* **292,** 111–123
32. Gundersen, G. G., Khawaja, S., and Bulinski, J. C. (1987) *J. Cell Biol.* **105,** 251–264
33. Wishart, D. S., Bigam, C. G., Holm, A., Hodges, R. S., and Sykes, B. D. (1995) *J. Biomol. NMR* **5,** 67–81
34. Al-Bassam, J., Ozer, R. S., Safer, D., Halpain, S., and Milligan, R. A. (2002) *J. Cell Biol.* **157,** 1187–1196
35. Devred, F., Barbier, P., Douillard, S., Monasterio, O., Andreu, J. M., and Peyrot, V. (2004) *Biochemistry* **43,** 10520–10531
36. Chau, M. F., Radeke, M. J., de Inés, C., Barasoain, I., Kohlstaedt, L. A., and Feinstein, S. C. (1998) *Biochemistry* **37,** 17692–17703
37. Sillen, A., Barbier, P., Landrieu, I., Lefebvre, S., Wieruszeski, J. M., Leroy, A., Peyrot, V., and Lippens, G. (2007) *Biochemistry* **46,** 3055–3064
38. Landino, L. M., Skreslet, T. E., and Alston, J. A. (2004) *J. Biol. Chem.* **279,** 35101–35105
39. Wolff, J. (1998) *Biochemistry* **37,** 10722–10729
40. Mechulam, A., Chernov, K. G., Mucher, E., Hamon, L., Curmi, P. A., and Pastré, D. (2009) *PLoS Comput. Biol.* **5,** e1000255
41. Kar, S., Florence, G. J., Paterson, I., and Amos, L. A. (2003) *FEBS Lett.* **539,** 34–36
42. Joe, P. A., Banerjee, A., and Ludueña, R. F. (2009) *J. Biol. Chem.* **284,** 4283–4291
43. Luchko, T., Huzil, J. T., Stepanova, M., and Tuszynski, J. (2008) *Biophys. J.* **94,** 1971–1982
44. Wang, Z., and Sheetz, M. P. (2000) *Biophys. J* **78,** 1955–1964
45. White, S. R., Evans, K. J., Lary, J., Cole, J. L., and Lauring, B. (2007) *J. Cell Biol.* **176,** 995–1005
46. Tompa, P. (2002) *Trends Biochem. Sci.* **27,** 527–533
47. Ackmann, M., Wiech, H., and Mandelkow, E. (2000) *J. Biol. Chem.* **275,** 30335–30343
48. Nogales, E., Whittaker, M., Milligan, R. A., and Downing, K. H. (1999) *Cell* **96,** 79–88
49. Mukrasch, M. D., Bibow, S., Korukottu, J., Jeganathan, S., Biernat, J., Griesinger, C., Mandelkow, E., and Zweckstetter, M. (2009) *PLoS Biol.* **7,** e34
50. Mukrasch, M. D., von Bergen, M., Biernat, J., Fischer, D., Griesinger, C., Mandelkow, E., and Zweckstetter, M. (2007) *J. Biol. Chem.* **282,** 12230–12239
51. Fernández, C. O., Hoyer, W., Zweckstetter, M., Jares-Erijman, E. A., Subramaniam, V., Griesinger, C., and Jovin, T. M. (2004) *EMBO J.* **23,** 2039–2046
52. Igarashi, K., and Kashiwagi, K. (2010) *Int. J. Biochem. Cell Biol.* **42,** 39–51
53. Patel, M. M., and Anchordoquy, T. J. (2005) *Biophys. J.* **88,** 2089–2103
54. Ouameur, A. A., and Tajmir-Riahi, H. A. (2004) *J. Biol. Chem.* **279,** 42041–42054
55. Osawa, M., Yokogawa, M., Muramatsu, T., Kimura, T., Mase, Y., and Shimada, I. (2009) *J. Biol. Chem.* **284,** 26117–26126
56. Job, D., Fischer, E. H., and Margolis, R. L. (1981) *Proc. Natl. Acad. Sci. U.S.A.* **78,** 4679–4682
57. Schliwa, M., Euteneuer, U., Bulinski, J. C., and Izant, J. G. (1981) *Proc. Natl. Acad. Sci. U.S.A.* **78,** 1037–1041
58. Lobert, S., Hennington, B. S., and Correia, J. J. (1993) *Cell Motil. Cytoskeleton* **25,** 282–297
59. Doi, H., Kawaguchi, M., and Timasheff, S. N. (2003) *Biosci. Biotechnol. Biochem.* **67,** 1643–1652
60. Grabarek, Z. (2006) *J. Mol. Biol.* **359,** 509–525
61. Jia, J., Tarabykina, S., Hansen, C., Berchtold, M., and Cygler, M. (2001) *Structure* **9,** 267–275
62. Chenal, A., Guijarro, J. I., Raynal, B., Delepierre, M., and Ladant, D. (2009) *J. Biol. Chem.* **284,** 1781–1789
63. Meier, R., Drepper, T., Svensson, V., Jaeger, K. E., and Baumann, U. (2007) *J. Biol. Chem.* **282,** 31477–31483
64. Job, D., Pabion, M., and Margolis, R. L. (1985) *J. Cell Biol.* **101,** 1680–1689
65. Boucher, D., Larcher, J. C., Gros, F., and Denoulet, P. (1994) *Biochemistry* **33,** 12471–12477
66. Larcher, J. C., Boucher, D., Lazereg, S., Gros, F., and Denoulet, P. (1996) *J. Biol. Chem.* **271,** 22117–22124